

Effect of 3-Aminopropyltrimethoxysilane on Chemically Modified Oil Palm Mesocarp Fiber/Poly(butylene succinate) Biocomposite

Yoon Yee Then,^a Nor Azowa Ibrahim,^{a,*} Norhazlin Zainuddin,^a Buong Woei Chieng,^a Hidayah Ariffin,^b and Wan Md Zin Wan Yunus^c

Consecutive superheated steam-alkali treatment was introduced to modify oil palm mesocarp fiber (OPMF) prior to biocomposite fabrication. The biocomposite made up of 70 wt.% modified OPMF (SNOPMF) and 30 wt.% poly(butylene succinate) (PBS) was prepared by melt blending followed by compression molding. A silane coupling agent of 3-aminopropyltrimethoxysilane (APTMS) was also incorporated into the SNOPMF/PBS biocomposite during the compounding process to impart better adhesion at the SNOPMF-PBS interface. The experimental results revealed that the tensile, flexural, and impact strengths were enhanced by 16, 30, and 15%, respectively, after the introduction of 2 wt.% APTMS to the SNOPMF/PBS biocomposite. Similarly, the resistance to water uptake and thickness swelling of this biocomposite was improved by 34 and 49%, respectively, relative to SNOPMF/PBS biocomposite. The SEM observation of the tensile fracture surface showed that APTMS improved the interfacial adhesion between SNOPMF and PBS. Based on the results, it can be deduced that APTMS could be a good coupling agent for improving the SNOPMF-PBS adhesion and, thereby, lead to a water resistant biocomposite of enhanced mechanical properties.

Keywords: Biocomposite; Oil palm mesocarp fiber; Poly(butylene succinate); Silane; Alkali; Superheated steam

Contact information: a: Department of Chemistry, Faculty of Science, Universiti Putra Malaysia, 43400 UPM Serdang, Selangor, Malaysia; b: Department of Bioprocess Technology, Faculty of Biotechnology and Biomolecular Sciences, Universiti Putra Malaysia, 43400 UPM Serdang, Selangor, Malaysia; c: Department of Chemistry, Centre For Defence Foundation Studies, National Defence University of Malaysia, Sungai Besi Camp, 57000 Kuala Lumpur, Federal Territory of Kuala Lumpur, Malaysia; * Corresponding author: norazowa@upm.edu.my

INTRODUCTION

Recently, extensive research has been done on the utilization of natural fibers including oil palm (Teh *et al.* 2013; Then *et al.* 2013, 2014a,b, 2015a,b; Eng *et al.* 2014), kenaf (Mohd Sis *et al.* 2013), hemp (Terzopoulou *et al.* 2014), coir (Islam *et al.* 2010; Nam *et al.* 2011), rice straw (Zhao *et al.* 2012), and banana (Pothan *et al.* 2006) fibers as filler or reinforcements in fabricating of biocomposites, in place of synthetic fibers. These natural fibers show tremendous advantages relative to synthetic fibers, particularly due to their relatively lower density and production cost, in combination with their renewable, sustainable, and biodegradable characteristics (Terzopoulou *et al.* 2014). These natural fibers are made up of three main components, namely cellulose, hemicellulose, and lignin, which are responsible for their physical and mechanical properties and are varied depending on the origin of the fibers (Georgopoulos *et al.* 2005). The broad availability

and ease of processing of natural fibers has made them a desirable substitute for synthetic fibers in the biocomposite industry (Pothan *et al.* 2006).

It is well known that oil palm is one of the prime industrial crops in Malaysia along with rubber and pepper. This has given rise to Malaysia becoming the second largest palm oil producer in the world after Indonesia. In the palm oil industry, only 10% of the oil palm tree is used for oil production and the remaining 90% is biomass, which is normally dumped in either the plantation area or oil palm mills (Basiron 2007). The remaining oil palm biomass has great potential to be further utilized as a filler or reinforcement in biocomposite applications. Among biomasses, oil palm mesocarp fiber (OPMF) is of interest here due to its abundance as well as its availability at almost zero cost, after extraction of crude palm oil from oil palm fruits (Sreekala *et al.* 1997). Oil palm mesocarp fiber is normally burnt as a solid fuel to self-supply the steam and electricity required for the operation of the mill and is under-utilized commercially (Lau *et al.* 2008). Efforts are already being made for producing value added product, particularly for biocomposite materials, from this biomass (Teh *et al.* 2013; Then *et al.* 2013, 2014a,b, 2015a,b; Eng *et al.* 2014).

Poly(butylene succinate) (PBS) is a biodegradable thermoplastic synthesized *via* a poly-condensation process, using succinic acid and 1,4-butanediol as monomers (Kim *et al.* 2006). It has a relatively low processing temperature of roughly 120 °C, and is therefore suitable for use in fabricating natural fiber-filled thermoplastic biocomposites, in which degradation to fiber, occurring at roughly 160 °C, could be minimized during the compounding process. In addition to its biodegradability and relatively low processing temperature, PBS is also available at lower prices than other biodegradable thermoplastics such as polylactic acid and polyhydroxybutyrate (Nam *et al.* 2011). These features have made PBS a suitable candidate to be compounded with natural fiber for developing price competitive biocomposite materials.

Nowadays, many interior and exterior parts of car compartments are made from natural fiber biocomposite materials due to the interesting properties of natural fibers such as light weight, low production cost and energy, ecological sustainable, and biodegradable as well as carbon dioxide neutral (Terzopoulou *et al.* 2014). Therefore, there is no doubt that the biocomposites made of PBS and OPMF may have showed potential application in automotive market.

In general, OPMF and PBS have very different properties; one is hydrophilic whilst another is hydrophobic. As a result, the biocomposites made of OPMF and PBS normally have poor mechanical properties, attributing to their weak interfacial adhesion (Then *et al.* 2013). A number of different techniques can be used to enhance the interfacial properties of a biocomposite, including surface modification of fiber as well as the introduction of a third component, normally referred to as a coupling agent, to the biocomposite (Mohd Sis *et al.* 2013; Teh *et al.* 2013). In authors' previous reports, OPMF was surface modified using superheated steam and alkali treatments (Then *et al.* 2014c). These treatments have proven to enhance the wettability of fiber surfaces by thermoplastic, which in turn improved the mechanical properties and dimensional stability of the corresponding biocomposite (Then *et al.* 2014a, 2015a,b). However, those treatments can only partially remove the hemicellulose component in fiber, and that remaining hemicellulose component can hinder the performance of the biocomposite.

In the present study, OPMF was pre-treated using consecutive superheated steam-alkali treatments, aiming to substantially remove residual hemicellulose as well as to increase the accessibility of the fiber's hydroxyl groups toward the silane coupling agent

in the subsequent compounding process for biocomposite preparation. Silane, which is normally used as a coupling agent, has bi-functional structures which may respectively react with the fiber and thermoplastic, forming a chemical linkage between them (Xie *et al.* 2010). A number of different amino-silane coupling agents have been investigated for improving adhesion between natural fibers and thermoplastics (Zhao *et al.* 2012; Mohd Sis *et al.* 2013). According to Mohd Sis *et al.* (2013), the addition of 2 wt.% 3-aminopropyltrimethoxysilane (APTMS) to a biocomposite of PLA/polybutylene adipate-co-terephthalate/kenaf fiber results in an increase of tensile, flexural, and impact strengths.

In the present study, APTMS was chosen to be used as a coupling agent for improving fiber-thermoplastic adhesion, due to its relative non-toxicity and high boiling point. The effect of APTMS addition on dimensional stability as well as mechanical, morphological, and thermal properties of superheated steam-alkali-treated OPMF/PBS biocomposite was reported.

EXPERIMENTAL

Materials

Oil palm mesocarp fiber (OPMF) was collected from FELDA Serting Hilir Oil Palm Mill (Malaysia). Before use, it was washed by being soaked in distilled water at 25 °C for 24 h, rinsed with hot water at 60 °C followed by acetone, and was finally oven-dried at 60 °C. This process was carried out to remove dirt adhered to the fibers' surface, as well as some oil residues. The dried fiber was then ground and sieved to obtain particles with sizes between 150 to 300 µm for use in chemical treatment as well as for biocomposite preparation. Poly(butylene succinate) (PBS), under the trade name of BIONOLLE™ 1903MD, was supplied by Showa Denko (Japan). It has a density of 1.26 g/cm³ and a melting point of approximately 115 °C. Its molecular structure is shown in Fig. 1. The 3-aminopropyltrimethoxysilane (APTMS) with 97% assay was purchased from Sigma-Aldrich (USA) and used as received. It appears as colorless liquid with a density of 1.03 g/cm³ and a boiling point of 194 °C. The molecular structure of APTMS is illustrated in Fig. 2. Analytical grade sodium hydroxide (NaOH) pellets were purchased from Merck (Germany) and used as received.

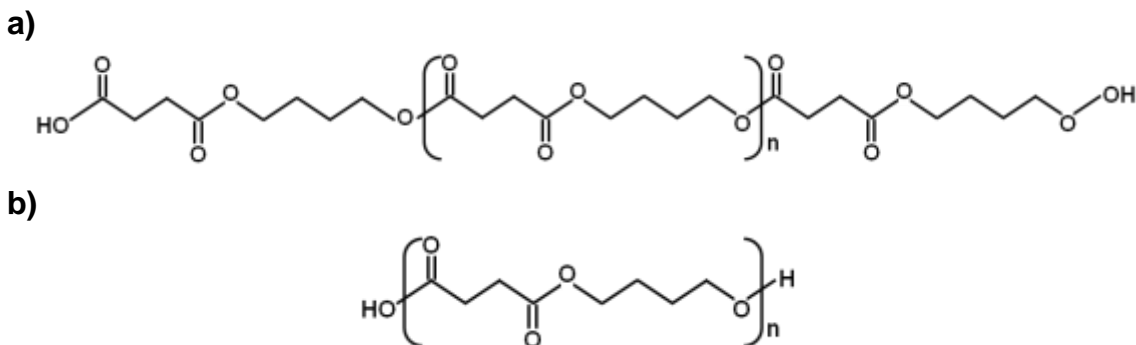


Fig. 1. (a) Molecular structure of PBS and (b) its repeating unit

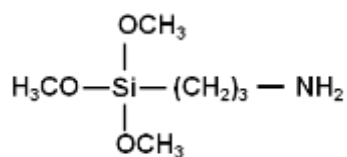


Fig. 2. Molecular structure of APTMS

Methods

Modification of OPMF

The modification of OPMF was carried out according to the method previously described by Then *et al.* (2014c). In brief, OPMF was first pre-treated in a superheated steam oven at a temperature of 220 °C for 60 min and subsequently soaked in 2% NaOH solution for 3 h at room temperature. The weight ratio of fiber-to-NaOH solution was fixed at 1:20. After treatment, the fiber was filtered and washed several times with water, oven-dried at 60 °C, and finally kept in a sealed polyethylene bag for use in biocomposites fabrication. This treated fiber was labeled as SNOPMF. The properties of OPMF and SNOPMF are given in Table 1 (Then *et al.* 2014c).

Table 1. Chemical Compositions and Crystallinity of Fibers

Fibers	Cellulose (%)	Hemicellulose (%)	Lignin (%)	Moisture (%)	Crystallinity (%)
OPMF	32.22	31.62	23.89	7.87	33.0
SNOPMF	47.52	5.27	36.82	2.49	45.6

Fabrication of biocomposites

The OPMF, SNOPMF, and PBS were oven-dried at 60 °C prior to the compounding process. Biocomposites of SNOPMF/PBS/APTMS were fabricated by melt mixing of SNOPMF, PBS, and 2 wt.% APTMS in a Brabender internal mixer (Germany) at 120 °C with a rotor speed of 50 rpm for 15 min (Then *et al.* 2013). The wt.% of APTMS was calculated according to the weight of its fiber and that the weight ratio of fiber-to-PBS was fixed at 70:30.

In summary, PBS pellets were first melted in the Brabender mixing chamber for 2 min. Next, fiber was slowly added into the molten PBS and mixing continued for another 2 min. After that, the pre-weighed amount of APTMS was directly added into the mixing chamber and mixing was continued for a total time of 15 min. Apart from that, biocomposites of OPMF/PBS and SNOPMF/PBS at weight ratios of 70:30 were also prepared as the standard samples for comparison. The compounded material was compressed by hydraulic hot-press at temperature of 120 °C for 5 min under pressure of 150 kgf/cm² into sheets with thicknesses of 1- and 3-mm, and it was subsequently cold-pressed at a temperature of 30 °C for 5 min. The abbreviations used for the biocomposites are shown in Table 2.

Table 2. Abbreviations used for Biocomposites

Abbreviation	PBS (wt.%)	OPMF (wt.%)	SNOPMF (wt.%)	APTMS (wt.%)
OPMF/PBS	30	70	-	-
SNOPMF/PBS	30	-	70	-
SNOPMF/PBS/APTMS	30	-	70	2

Mechanical properties measurements

Tensile testing was carried out on the biocomposites by using a Universal Testing Machine, Instron-4302 (USA) equipped with a 1 kN load cell. The test specimens were cut into dumbbell shapes from 1-mm sheets as specified by the American Society of Testing and Materials (ASTM) D638-5 (2000). The test was conducted at 25 °C with a crosshead speed of 5 mm/min. Instron Series IX software was implemented to determine the tensile strength, tensile modulus, and elongation at break.

A three points bending flexural test was conducted on the biocomposites by using a Universal Testing Machine, Instron-4302 (USA) equipped with a 1 kN load cell, as described in ASTM D790 (2000) standard. Rectangular test specimens with dimensions of 127.0 mm × 12.7 mm × 3.0 mm (length × width × thickness) were cut from the 3-mm sheets for testing. The test was conducted at 25 °C with a crosshead speed of 1.3 mm/min and a span length of 48 mm. The results were expressed in terms of flexural strength and flexural modulus, as determined using Instron Series IX software.

Un-notched Izod impact testing was carried out on the biocomposites by using an IZOD Impact Tester (India) equipped with a 7.5 J pendulum at 25 °C, based on ASTM D256 (2000) standard. The test specimens were cut to dimensions of 64.0 mm × 12.7 mm × 3.0 mm. The impact strength (J/m) was calculated by dividing the energy (J) needed to break the specimen over the thickness (m) of specimen.

The above tests were performed on five specimens for each formulation, and the average values and standard deviations were reported.

Interfacial properties

The scanning electron micrographs of OPME, SNOPME, and tensile fracture surfaces of the biocomposites were recorded by using a JEOL JSM-6400 scanning electron microscope (Japan) operated at 15 kV accelerating voltage. The oven-dried samples were placed on the metal holder and coated with gold by a Bio-Rad sputter coater (USA) for 3 min to ensure good conductivity prior to analysis.

A short beam shear (three point bending) test was conducted on the biocomposites according to the ASTM D2344 (2000) standard by using a Universal Testing Machine-Instron 4302 (USA) equipped with a 1 kN load cell. The test specimens were cut to dimensions of 25.0 mm × 12.7 mm × 3.0 mm. The test was performed at 25 °C with a constant crosshead speed of 1.3 mm/min and span length of 15 mm. The result was expressed in terms of apparent interlaminar shear strength as determined using Instron Series IX software. The test was performed on five specimens for each formulation, and the average values and standard deviations were reported.

Fourier transform infrared (FTIR) spectroscopy

The functional groups and types of bonding of the biocomposites were identified by using a Perkin Elmer Spectrum 100 series spectrophotometer (USA) equipped with attenuated total reflectance (ATR) capability. The FTIR spectra for the biocomposites were recorded over a range of frequencies from 400 to 4000 cm⁻¹ with 16 scans in each case at a resolution of 4 cm⁻¹.

Dimensional stability

The dimensional stability of the biocomposites was assessed *via* water absorption and thickness swelling tests; these tests were conducted according to the ASTM D570 standard (2005) and European EN 317 (2003) standard, respectively. Testing specimens

with the dimensions 10.0 mm × 10.0 mm × 1.0 mm were cut from the 1-mm sheets. Prior to testing, the specimens were oven-dried at 60 °C until a constant weight was reached. The initial weight (W_i) and thickness (T_i) of the dried specimens were measured using a microbalance and a caliper, respectively. The specimens were then immersed in distilled water for 24 h at 25 °C. After that, the specimens were removed from the distilled water and wiped with tissue paper to remove excess water from their surfaces. The final weights (W_f) and thicknesses (T_f) of the specimens were measured immediately. The tests were performed in duplicate, and the average values and standard deviations were reported. The water absorption, as well as the thickness swelling of the biocomposites was calculated following Eqs. 1 and 2, respectively:

$$\text{Water Absorption (\%)} = \frac{W_f - W_i}{W_i} \times 100 \quad (1)$$

$$\text{Thickness Swelling (\%)} = \frac{T_f - T_i}{T_i} \times 100 \quad (2)$$

Dynamic mechanical analysis (DMA)

The dynamic mechanical properties of PBS and its biocomposites were examined according to the ASTM D5023 (2009) standard, by using a Perkin-Elmer PYRIS Diamond dynamic mechanical analyzer (USA) with bending mode. The dimensions of the specimens used were of 40 mm × 13 mm × 1 mm. The temperature scan was from -80 to 50 °C at a constant heating rate of 10 °C/min with a frequency of dynamic force of 1 Hz, under a nitrogen atmosphere. The storage modulus (E') and damping properties ($\tan \delta$) of each specimen were recorded as a function of temperature.

Differential scanning calorimetric (DSC) analysis

The melting and crystallization behaviors of PBS and its biocomposites were studied by using a Perkin Elmer JADE DSC differential scanning calorimeter (USA) in accordance with the ASTM D3418 (2008) standard. The weight of the samples used ranged from around 8 to 10 mg. The samples were first heated from 60 to 130 °C with a heating rate of 10 °C/min, and kept at this temperature for 3 min to remove the thermal history of the samples. The samples were then cooled down to 60 °C with the cooling rate of 10 °C/min, to allow the samples to dynamically crystallize, and kept at this temperature for 3 min. Subsequently, the crystallized samples were then re-heated up to 130 °C with the heating rate of 10 °C/min. All the heating and cooling scans run in the melting and crystallization studies were carried out under a nitrogen (N_2) atmosphere at a flow rate of 20 mL/min to prevent oxidation of the samples. The percentage crystallinity index (χ_c), was calculated from the second melting enthalpy values using the following relationship (Eq. 3),

$$\chi_c = \frac{\Delta H_m}{\alpha \Delta H_m^0} \times 100 \quad (3)$$

where ΔH_m is the melting enthalpy of the samples (J/g), ΔH_m^0 is the enthalpy value of the melting of a 100% crystalline form of PBS (110.3 J/g), and α is the weight fraction of thermoplastics in the biocomposite materials.

Thermogravimetric analysis (TGA)

Thermal degradation behaviors of the biocomposites were studied by using a Perkin Elmer Pyris 7 TGA analyzer within a temperature range of 35 to 500 °C at a constant heating rate of 10 °C/min and continuous nitrogen flow of 20 mL/min. The weights of the samples used were from 10 to 15 mg. The weight losses of the samples were recorded as a function of temperature.

RESULTS AND DISCUSSION

Mechanical Properties

In this study, the mechanical properties of the biocomposites were characterized *via* tensile, flexural, and impact tests. The examination of the mechanical properties of the biocomposites can be used to qualify the adhesion at the interface of the fibers and the thermoplastic. Generally, stronger adhesion strength results in biocomposites with higher mechanical properties (Vilaseca *et al.* 2008).

The tensile strength, modulus, and strain of OPMF/PBS, SNOPMF/OPMF, and SNOPMF/PBS/APTMS biocomposites are summarized in Table 3. As reported in a previous work (Then *et al.* 2013), the tensile strength, modulus, and strain of neat PBS were 37.31 MPa, 248.90 MPa, and 470.00%, respectively. It can be noted that the introduction of 70 wt.% OPMF to PBS (OPMF/PBS) drastically decreased the initial tensile strength, modulus, and strain of PBS to 13.86 MPa, 94.80 MPa, and 2.50%, respectively. Similar results have been published by Georgopoulos *et al.* (2005), who studied the properties of low density polyethylene/natural fiber composites. The decrease in tensile properties could be due to inefficient stress transfer across the PBS-OPMF interface when a load was applied to the biocomposite, resulting from inadequate interfacial adhesion between the two phases. Apart from that, the impurities present on the surface of OPMF (Fig. 3a) could also hinder the adhesion characteristic of the fiber's polymer matrix, thereby reducing stress transfer efficiency. Additionally, fibers also tend to agglomerate, especially at high loading, due to the increase in fiber-fiber interactions, which can result in regions of stress concentration and decrease the energy required to break (Karmarkar *et al.* 2007).

Table 3. Tensile Properties of Biocomposites

Sample	Tensile		
	Strength (MPa)	Modulus (MPa)	Strain (%)
PBS	37.31 ± 0.91	248.90 ± 4.40	470.00 ± 55.20
OPMF/PBS	13.86 ± 0.73	94.80 ± 7.60	2.50 ± 0.29
SNOPMF/PBS	23.44 ± 0.25	670.80 ± 25.60	3.40 ± 0.14
SNOPMF/PBS/APTMS	27.12 ± 1.21	869.00 ± 25.72	3.90 ± 0.13

Data presented as the mean ± standard deviation

It is interesting to note that the pre-treatment of fiber with superheated steam and alkali (SNOPMF) had considerably improved the tensile strength, modulus, and strain for the SNOPMF/PBS biocomposite in comparison to that of the OPMF/PBS biocomposite, as can be seen in Table 3. The increment in tensile strength, modulus, and strain for the SNOPMF/PBS biocomposite were recorded to be 69, 608, and 36%, relative to the OPMF/PBS biocomposite. It has been demonstrated that the pre-treatment process

renders the fiber surface relatively clean and coarse (Fig. 3b), providing better adhesion and increasing the number of sites available for mechanical interlocking with PBS, ultimately resulting in stronger interfacial adhesion within the biocomposite. Additionally, the decrease in the hemicellulose percentage, as well as the increase in the percentages of cellulose and crystallinity for SNOPMF (Table 1) also boosted the effectiveness of the fiber as reinforcement within the biocomposite (Bachtiar *et al.* 2008). Those features, in turn, gave rise to a biocomposite of relatively higher tensile properties.

Furthermore, the addition of 2 wt.% APTMS to the SNOPMF/PBS biocomposite has continued to boost the tensile properties of the corresponding biocomposite. As can be seen from Table 3, the tensile strength, modulus, and strain of the SNOPMF/PBS/APTMS biocomposite were of 27.12 MPa, 869.00 MPa, and 3.90%, respectively. The tensile strength, modulus, and strain of the SNOPMF/PBS/APTMS biocomposite were respectively 16, 30, and 15% higher than that of the SNOPMF/PBS biocomposite. The enhancement in tensile properties for the SNOPMF/PBS/APTMS biocomposite can be explained by the fact that APTMS can promote the dispersion of fiber within the biocomposite as well as assist in coupling the SNOPMF and PBS together *via* chemical linkage, resulting in a biocomposite with relatively uniform fiber dispersion and stronger bonding strength, in turn producing a biocomposite with enhanced tensile properties. This will be further discussed in the sections of microscopy examination and Fourier transform infrared spectroscopy.

The flexural strength, modulus, and impact strength of the biocomposites discussed here are tabulated in Table 4. Similar to the tensile behaviors, the presence of OPMF has decreased the flexural strength of neat PBS by 27%, to a value of 27.26 MPa. Nevertheless, the flexural strength was increased to 37.79 MPa for the SNOPMF/PBS biocomposite, with 39% increment recorded. The introduction of 2 wt.% APTMS to the SNOPMF/PBS biocomposite resulted in further enhancement of flexural strength by 24%, achieving a value of 46.92 MPa. It is of note that the flexural strength of the SNOPMF/PBS/APTMS biocomposite was nearly 25% higher than that of neat PBS. The improvement in flexural strength can be attributed to the improved interfacial adhesion and uniform dispersion of fiber within the biocomposite (Vilaseca *et al.* 2008). On the other hand, the initial flexural modulus of neat PBS was increased from 562.90 MPa to 2191.00 MPa for the OPMF/PBS biocomposite. This value is 289% higher than that of neat PBS. The flexural modulus was further increased by 46% as the OPMF was substituted with SNOPMF for the SNOPMF/PBS biocomposite. The addition of APTMS to the SNOPMF/PBS biocomposite only caused a marginal increase in the flexural modulus. According to Wang *et al.* (2014), the improvement in flexural modulus could be caused by the relatively high stiffness of fibers that are well distributed within the biocomposite.

Table 4. Flexural Properties and Impact Strength of Biocomposites

Sample	Flexural		Impact strength (Jm ⁻¹)
	Strength (MPa)	Modulus (MPa)	
PBS	37.58 ± 0.56	562.90 ± 42.90	416.96 ± 21.45
OPMF/PBS	27.26 ± 0.99	2191.00 ± 96.00	65.75 ± 3.08
SNOPMF/PBS	37.79 ± 0.79	3194.00 ± 32.00	76.93 ± 1.83
SNOPMF/PBS/APTMS	46.92 ± 1.45	3243.00 ± 98.00	83.26 ± 1.56

Data presented as the mean ± standard deviation

The plastic-like nature of neat PBS can absorb more impact energy and has a high impact strength of 416.96 Jm^{-1} , as shown in Table 4. However, the melt mixing of PBS and OPMF turned the behavior of PBS from flexible to brittle, as is indicated by a decreasing of impact strength to a value of 65.75 Jm^{-1} with 84% reduction recorded. However, after modifying the fiber surface properties as well as the introduction of APTMS, the impact strength was increased to 76.93 Jm^{-1} for SNOPMF/PBS biocomposite and 83.26 Jm^{-1} for SNOPMF/PBS/APTMS biocomposite. The improvement in impact strength was related to the improved ductility of the SNOPMF/PBS and SNOPMF/PBS/APTMS biocomposites, *i.e.*, higher value of tensile strain relative to OPMF/PBS biocomposite, which enabled them to absorb more impact energy before breaking. In addition, the relatively strong interfacial adhesion that developed in these biocomposite materials can also contribute to the delaying of crack initiation and propagation before failure and thereby improved its impact resistance. Similar observations were also reported by Vilaseca *et al.* (2008) in their study on recycled kraft fiber reinforced polypropylene biocomposites using maleated-polypropylene as a coupling agent.

Interfacial Properties

The changes in the microstructure of the fibers after treatment were viewed under scanning electron microscope and the microstructures of OPMF and SNOPMF are shown in Fig. 3. The micrographs show that the consecutive superheated steam-alkali treatment removed a considerable amount of impurities previously deposited on the surface of the OPMF (Fig. 3a), thus producing SNOPMF with a coarse surface texture (Fig. 3b). In addition, microfibrils that were previously embedded in the fiber bundle were largely exposed as a consequence of impurity and hemicellulose removals. The coarse surface as well as the exposure of SNOPMF microfibrils is of importance to increase the contact and adhesion between fiber and PBS, particularly via mechanical interlocking mechanism during biocomposite fabrication.

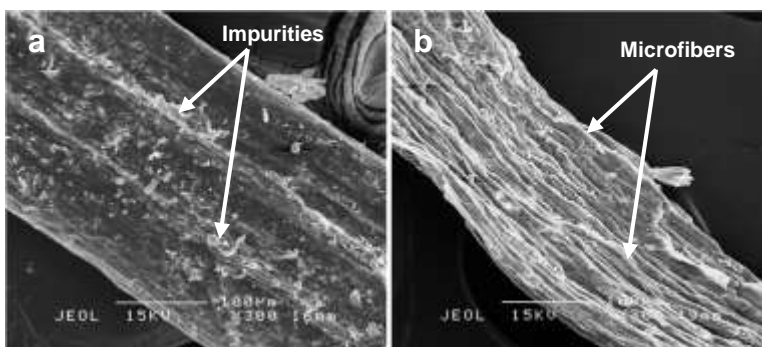


Fig. 3. Scanning electron micrographs of (a) OPMF and (b) SNOPMF

The comparisons of the tensile-fractured surfaces of the SNOPMF/PBS and SNOPMF/PBS/APTMS biocomposites with the OPMF/PBS biocomposite are shown in Fig. 4. These tensile-fractured surface micrographs can provide useful information regarding the failure mechanism under tensile load for the corresponding biocomposite. As can be seen in the micrograph of the OPMF/PBS biocomposite (Fig. 4a), the difference in the surface properties between hydrophilic OPMF and hydrophobic PBS has caused the fibers to interact poorly or distribute within the thermoplastic matrix and that

fibers are entangled to form fiber aggregates, resulting from fiber-fiber interaction (Xie *et al.* 2010). In addition, a visible gap can be seen at the OPMF-PBS interface region, which can be attributed either to the de-bonding mechanism during the tensile test or to poor adhesion between OPMF and PBS. Further, cavities also present resulting from fiber extraction during tensile testing. All of these characteristics are indications of poor adhesion between the OPMF and PBS, and explain the reduction in tensile, flexural, and impact strength.

The replacement of OPMF with SNOPMF changed the tensile fracture surface morphology of the corresponding biocomposite, as illustrated in Fig. 4b. The reduction in the hydrophilicity of SNOPMF, resulting from substantial removal of hemicellulose, increased its compatibility with the hydrophobic PBS. This was clearly manifested by the improvement of interfacial adhesion between SNOPMF and PBS where the fiber was closely packed with the PBS. Fewer cavities can be seen and their sizes are relatively smaller in comparison to that of the OPMF/PBS biocomposite. The distribution of fiber within the biocomposite was improved considerably, and fiber breakage could be seen. These observations indicate that better interfacial adhesion was developed in the SNOPMF/PBS biocomposite relative to the OPMF/PBS biocomposite.

The use of APTMS as a coupling agent further improved the wetting of SNOPMF by PBS and prevented the SNOPMF from dissociating from the PBS matrix. This is clearly manifested in the micrograph of the SNOPMF/PBS/APTMS biocomposite (Fig. 4c), where the surface fractures seem to be relatively flat and homogeneous, albeit fiber and thermoplastic were difficult to distinguish, and there was no indication of fiber dissociation after tensile testing. This indicated that APTMS could enhance the adhesion at the SNOPMF-PBS interface and subsequently improved the mechanical properties for the corresponding biocomposites, attributing to the increase of stress transfer efficiency from thermoplastic to fiber. This also explains the reason that the SNOPMF/PBS/APTMS biocomposite showed better tensile, flexural, and impact strength, relative to those of SNOPMF/PBS biocomposite as well as OPMF/PBS biocomposites.

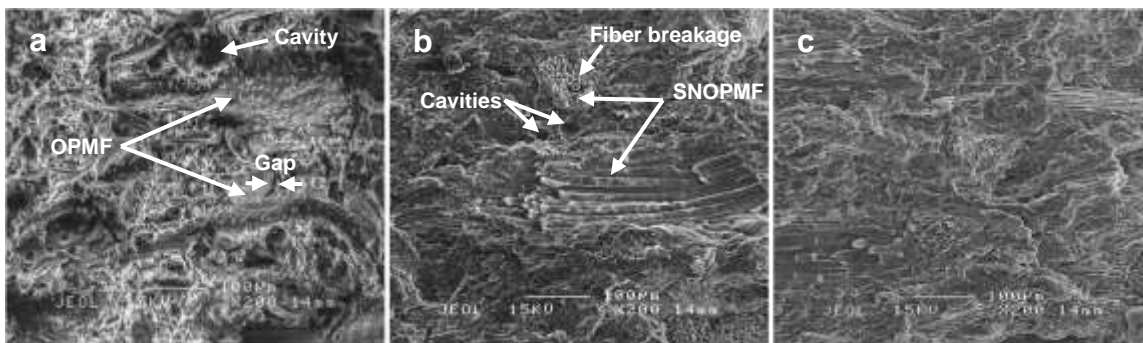


Fig. 4. Scanning electron micrographs of (a) OPMF/PBS, (b) SNOPMF/PBS, and (c) SNOPMF/PBS/APTMS biocomposites

The relatively strong interfacial adhesion between PBS and treated fibers, as discussed in the microscopy observations, can be quantified by a short beam shear test that measures the bonding strength between PBS and the OPMF and SNOPMF fibers. This relatively simple test involved loading a short sample under a three-point bending test such that interlaminar shear failure was induced and normally expressed as apparent

interlaminar shear strength (ILSS). The ILSS for OPMF/PBS, SNOPMF/PBS, and SNOPMF/PBS/APTMS biocomposites are plotted in Fig. 5.

The OPMF/PBS biocomposite showed a relatively low ILSS value of 1.64 MPa (Fig. 5), which was attributed to the poor interfacial adhesion at the OPMF-PBS interface, as is shown in the micrograph (Fig. 4a). The substitution of OPMF with SNOPMF increased the ILSS value to 3.30 MPa for the SNOPMF/PBS biocomposite. This value was 101% higher than that of the OPMF/PBS biocomposite, and the result is concurrent with microscopy observations and tensile test results, which showed improvement of interfacial adhesion between SNOPMF and PBS. The introduction of 2 wt.% APTMS into the SNOPMF/PBS biocomposite further enhanced the ILSS to a value of 4.74 MPa, showing 44% enhancement relative to the SNOPMF/PBS biocomposite. This ILSS enhancement can be attributed to the amino and alkoxy end groups of APTMS (Fig. 2) that are able to create a chemical linkage at the SNOPMF-PBS interface (Fig. 7e), thereby increasing the bonding strength between fiber and thermoplastic.

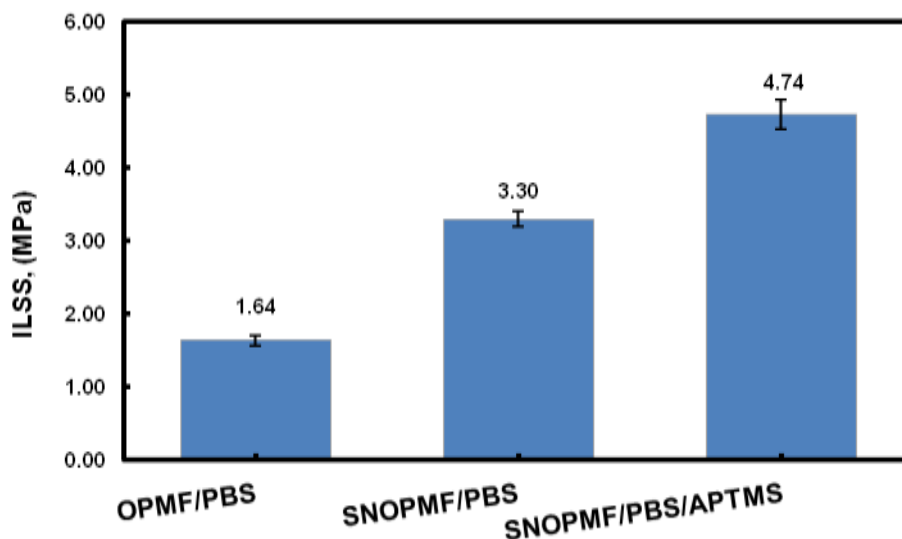


Fig. 5. Interlaminar shear strength of PBS/PBS, SNOPMF/PBS, and SNOPMF/PBS/APTMS biocomposites

Fourier Transform Infrared (FTIR) Spectroscopy

The FTIR spectra of the PBS, OPMF/PBS, SNOPMF/PBS, and SNOPMF/PBS/APTMS biocomposites are shown in Fig. 6.

The characteristic peaks of PBS can be seen at 3429, 2949, 1715, and 1170 cm^{-1} , corresponding to O-H stretching, C-H stretching, C=O stretching, and C-O-C stretching, respectively (Zhao *et al.* 2010). It is apparent that the absorption peaks in the spectra of the OPMF/PBS and SNOPMF/PBS biocomposites are identical to that of the PBS spectrum. There are no new peak formations or peak shifting, indicating that only physical interaction occurred within the biocomposite, mainly *via* a mechanical interlocking mechanism. It is interesting to note that the presence of 2 wt.% APTMS shifted the O-H stretching peak of SNOPMF/PBS from 3429 cm^{-1} to 3382 cm^{-1} , as illustrated in the spectrum of the SNOPMF/PBS/APTMS biocomposite. The other peaks remained identical to the PBS spectrum.

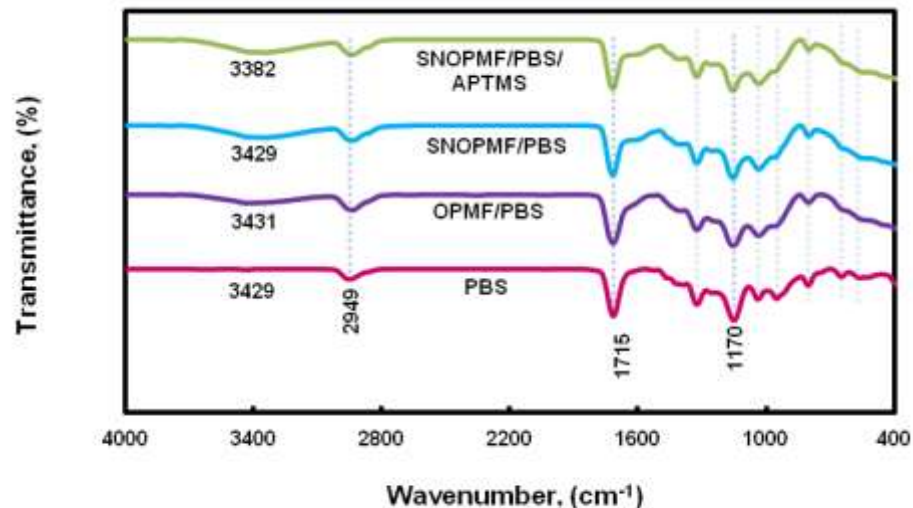
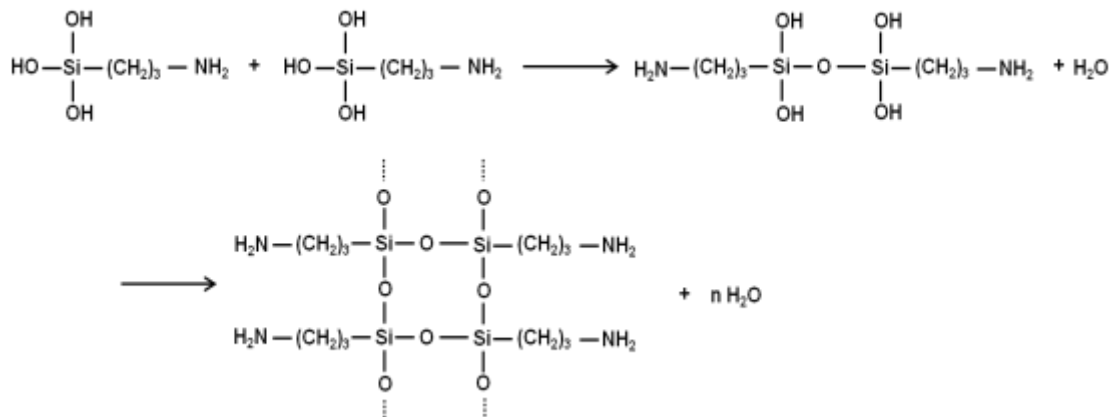


Fig. 6. FTIR spectra of PBS and its biocomposites

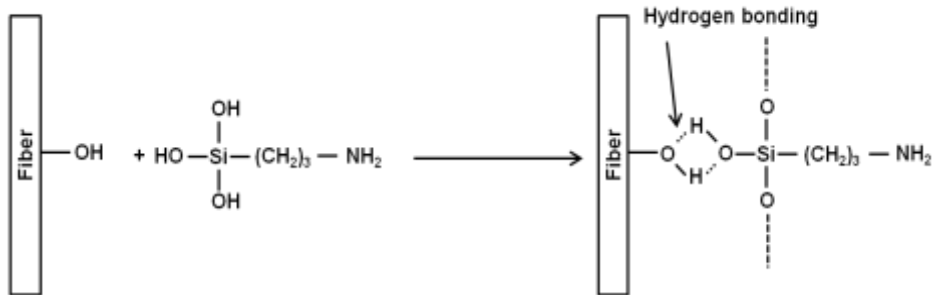
The peak shifting could be related to the hydrogen or covalent bonding interactions between hydrolyzed APTMS and the -OH groups in the fibers (Fig. 7c, d). It is suggested that the moisture present on the fiber can assist in the hydroxylation of the methoxy groups (-OCH₃) in the APTMS to form reactive silanol groups (-Si(OH)₃) (Fig. 7a). These silanol groups can then undergo self-condensation to form siloxane (-Si-O-Si-) (Fig. 7b), or interact with -OH groups in fibers to form hydrogen (Fig. 7c) or covalent bonding (Fig. 7d) (Zhao *et al.* 2012). The amino end group of APTMS had relatively high miscibility with PBS, thus there will be a possible reaction of this functional group with the carbonyl and -OH end groups of PBS *via* hydrogen bonding (Fig. 7e) (Nekkaa *et al.* 2012).



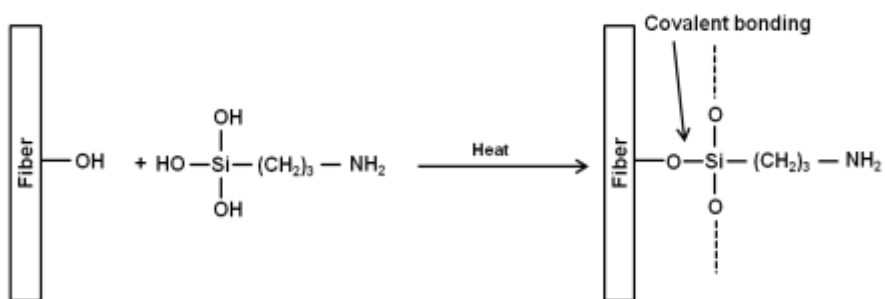
a) Hydrolysis of silane to silanol



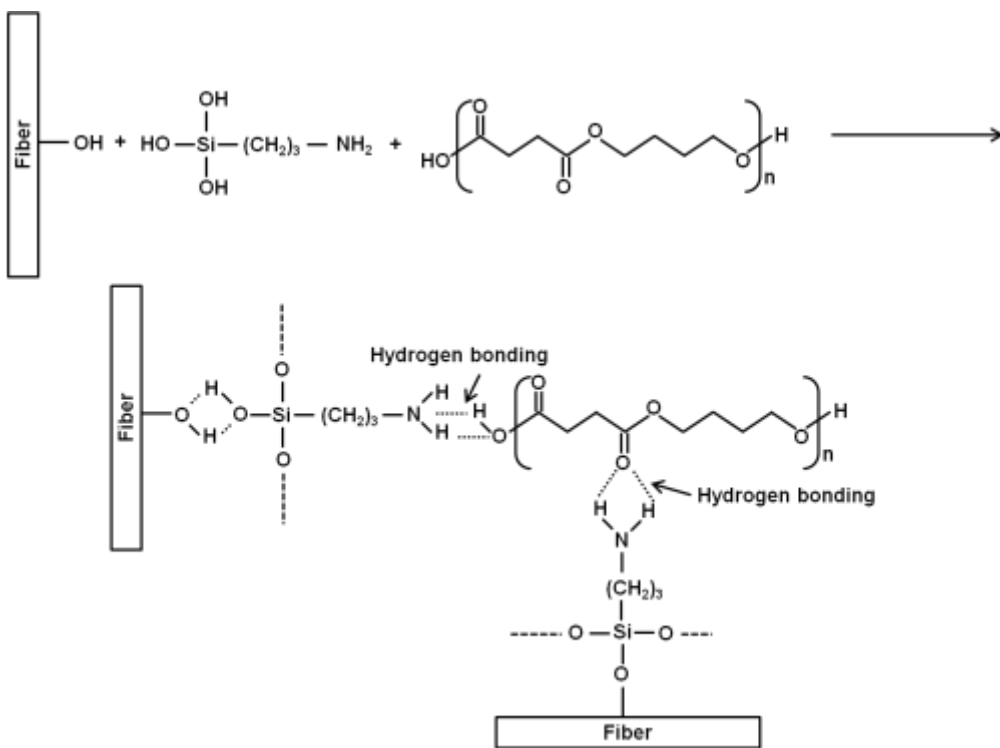
b) Self-condensation of silanol



c) Hydrogen bonding between fiber and silanol



d) Covalent bonding between fiber and silanol



e) Chemical linkage between fiber, silanol and PBS

Fig. 7. Schematic illustration of chemical reactions (a-e) between fiber, PBS, and APTMS

Dimensional Stability

The water uptake and thickness swelling of the PBS, OPMF/PBS, SNOPMF/PBS, and SNOPMF/PBS/APTMS biocomposites after 24 h of immersion in water are shown in Fig. 8. All of the biocomposites showed increases in water uptake and thickness swelling after 24 h of immersion in water, which was attributed to the presence of hydroxyl groups in the fibers which can induce moisture absorption (Islam *et al.* 2010). Natural fiber is hydrophilic in nature and readily absorbs water which results in fiber swelling, and that swelling of fiber can generate microcracks in the adjacent matrix and later act as a pathway for continuous penetration of water molecules via a capillary action. Apart from that, the hemicellulose component in natural fibers also contributes to water uptake due to the fact that hemicellulose is the most hydrophilic component in fiber and is the main contributor to the water absorption as compared to cellulose and lignin (Hosseinaei *et al.* 2012).

As can be seen in Fig. 8, the SNOPMF/PBS biocomposite showed a 61% reduction in water uptake and a 63% reduction in thickness swelling, in comparison to that of the OPMF/PBS biocomposite. This can be explained by the fact that SNOPMF has a lower percentage of hemicellulose (Table 1), which reduces its affinity to water absorption. In addition, the relatively strong interfacial adhesion at the SNOPMF-PBS interface, as well as the compact structure that developed within the SNOPMF/PBS biocomposite also restricted the penetration of water *via* microcracks in the adjacent matrix and subsequently reduced the water uptake and thickness swelling for the corresponding biocomposite. The presence of APTMS could further reduce the water uptake and thickness swelling for the SNOPMF/PBS/APTMS biocomposite by 34 and 49%, respectively, relative to the SNOPMF/PBS biocomposite. The reduction in water uptake and thickness swelling for the SNOPMF/PBS/APTMS biocomposite can be explained by the fact that part of the hydroxyl groups in SNOPMF are active in the formation of chemical linkage with APTMS, thus decreasing the number of hydroxyl groups that are available for interacting with water, which in turn can reduce the water uptake and thickness swelling.

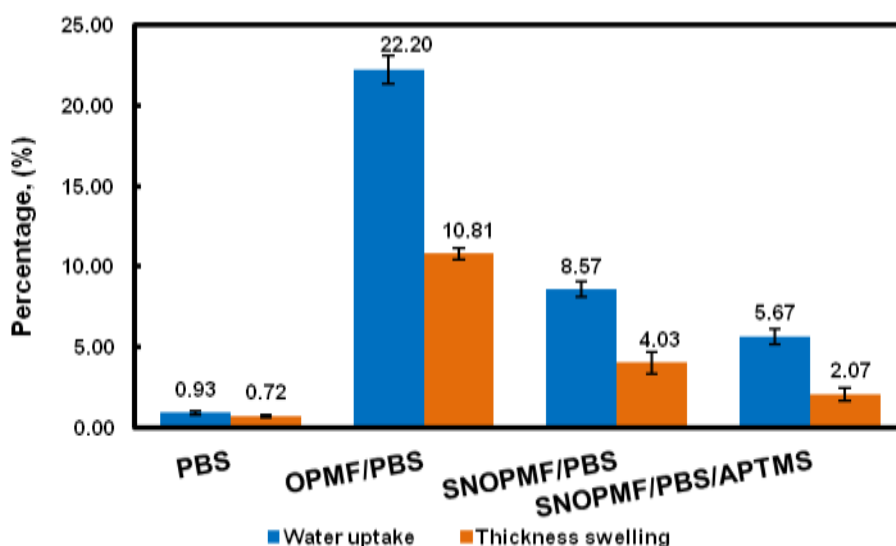


Fig. 8. Water uptake and thickness swelling of neat PBS and its biocomposites

Dynamic Mechanical Analysis

The thermo-mechanical behavior of the biocomposites was also determined *via* dynamic mechanical analysis. The storage modulus (E') of the biocomposites as a function of temperature at a frequency of 1 Hz is depicted in Fig. 9. The E' of neat PBS is also included in the figure as a reference. The E' is closely related to the load bearing capacity of a material and is analogous to the flexural modulus.

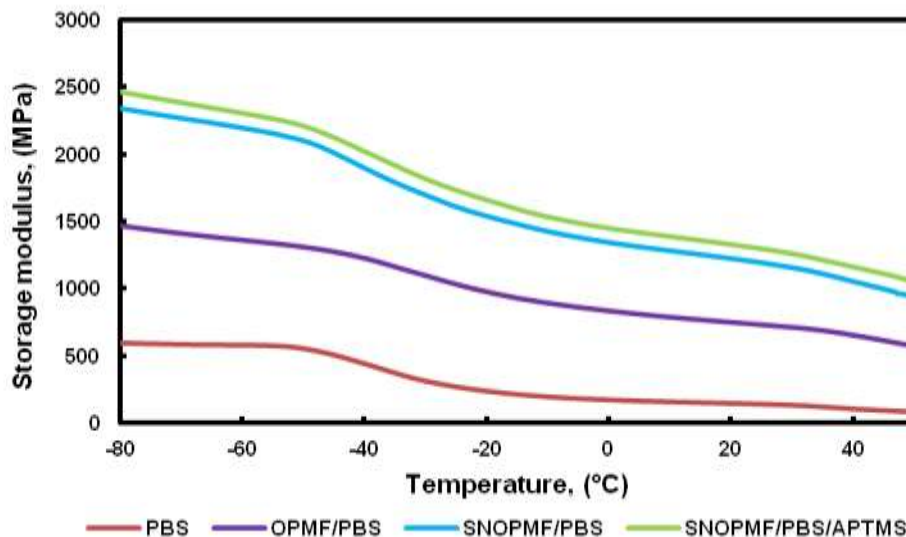


Fig. 9. Storage modulus of neat PBS and its biocomposites

Table 5. Storage Modulus (E'), Tan Delta, and Glass Transition Temperature (T_g) of PBS and Its Biocomposites

Sample	E' at -60.0 °C (MPa)	E' at 30.0 °C (MPa)	$\tan \delta$ at maximum peak height	T_g (°C)
PBS	578.95	127.69	1.26	-33.2
OPMF/PBS	1365.51	711.20	0.72	-28.6
SNOPMF/PBS	2199.16	1158.15	0.66	-32.5
SNOPMF/PBS/PBS	2306.36	1260.56	0.64	-33.9

It was clear from the results seen in Fig. 9 that the E' for both PBS and the biocomposites decreased with increasing temperature due to the increased chain mobility of polymeric materials at higher temperatures (Kim *et al.* 2005). As shown in Table 5, there was a drastic, almost 78% decrease in E' for PBS from 578.95 MPa at -60 °C to 127.69 MPa at 30.0 °C. A sharp drop in E' can be seen in the temperature range of -50.0 to -20.0 °C, which is associated with the glass transition temperature (T_g) of PBS. As compared to neat PBS, the biocomposites showed higher E' over the entire temperature range of the study. This may be attributed to the presence of fiber restricting the chain mobility of PBS, thereby stiffening the biocomposite and resulting in a higher E' . A similar observation was also reported by Bin *et al.* (2011) in PBS composites reinforced with cotton stalk bast fibers.

Among all the biocomposites herein studied, SNOPMF/PBS/APTMS showed the highest E' value for the entire temperature range of the study. For instance, the E' at 30 °C for the OPMF/PBS biocomposite was recorded as 711.20 MPa, and it increased to 1158.15 MPa and 1260.56 MPa for SNOPMF/PBS and SNOPMF/PBS/APTMS

biocomposites, respectively. This result is in line with the flexural modulus measurements previously reported. As was seen in the microscopy observation, the improved interfacial adhesion between SNOPMF and PBS could be the reason for this enhancement. It is of note that the SNOPMF/PBS/APTMS biocomposite showed a slightly higher storage modulus relative to SNOPMF/PBS biocomposite. This could be due to the chemical bonding mechanism in the presence of APTMS, as explained previously in FTIR study, which may lead to more efficient stress transfer from the thermoplastic to the fibers as well as an increase in E' .

The loss factor, normally denoted as $\tan \delta$, with respect to temperature for PBS and its biocomposites is plotted in Fig. 10. The $\tan \delta$ is taken as the ratio of loss modulus to storage modulus and reflecting the damping properties for the corresponding material. The variation of the $\tan \delta$ peak values of biocomposites is tabulated in Table 5 and represented as the y-axis value. The OPMF/PBS biocomposite showed a higher $\tan \delta$ peak value in comparison to those of SNOPMF/PBS and SNOPMF/PBS/APTMS biocomposites. The higher $\tan \delta$ peak value for OPMF/PBS biocomposite may be attributed to more energy being dissipated by internal friction at the relatively poor interface between OPMF and PBS. Normally, higher the $\tan \delta$ peak value indicates poor adhesion at the fiber-thermoplastic interface (Dong and Gauvin 1993).

Among the biocomposites, SNOPMF/PBS/APTMS showed the lowest $\tan \delta$ peak values. Since the $\tan \delta$ peak value is related to adhesion at the fiber-thermoplastic interface, the lower $\tan \delta$ peak value of SNOPMF/PBS/APTMS corresponds to better interfacial bonding and compatibility between SNOPMF and PBS in the presence of APTMS. This result is concurrent with microscopy observation and mechanical properties measurement. A similar observation was also reported by Pothan *et al.* (2003) in banana fiber reinforced polyester composites.

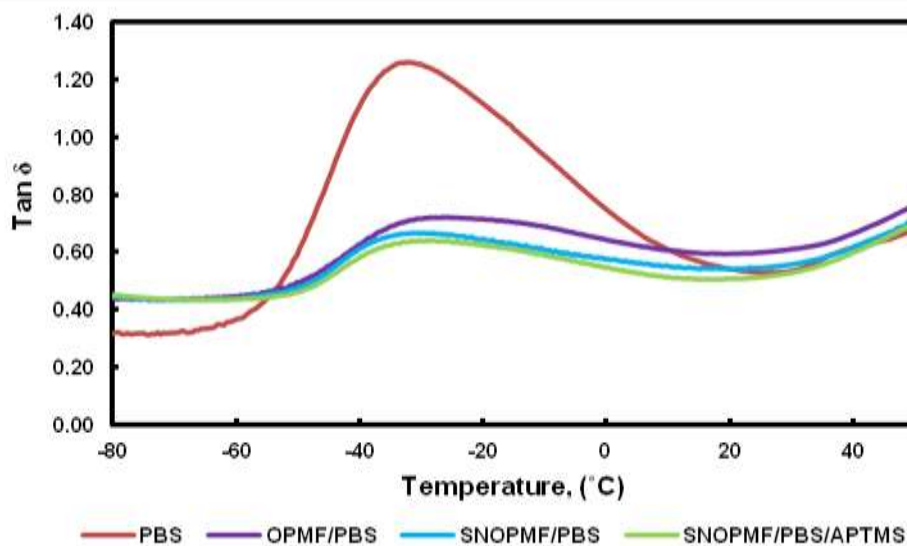


Fig. 10. Loss factor of neat PBS and its biocomposites

The glass transition temperatures (T_g) corresponded with the $\tan \delta$ curves, represented by the x-axis value, which were -28.6, -32.5, and -33.9 °C, respectively, for the OPMF/PBS, SNOPMF/PBS, and SNOPMF/PBS/APTMS biocomposites. Compared to the OPMF/PBS biocomposite, a slight decrease in T_g was observed for the SNOPMF/PBS and SNOPMF/PBS/APTMS biocomposites. The uniform distribution of

fiber in the biocomposites, resulting from fiber treatment as well as the introduction of APTMS, could increase the flexibility and tensile strain value of biocomposites. This data indicates an increase in chain movement, resulting in the observed T_g decrease. A similar observation was reported by Ray *et al.* (2010) in alkali-treated sesame husk reinforced unsaturated polyester.

Differential Scanning Calorimetry

Differential scanning calorimetry (DSC) measures the amount of heat energy absorbed or released when a material is heated or cooled. It is a very useful technique to study thermal behaviors such as melting temperature and crystallization temperature. The DSC heating and cooling curves of neat PBS, OPMF/PBS, SNOPMF/PBS, and SNOPMF/PBS/APTMS biocomposites are shown in Figs. 11 and 12, respectively. Their first melting temperature (T_{m1}), second melting temperature (T_{m2}), enthalpy of melting (ΔH_m), crystallinity (χ_c), crystallization temperature (T_c), and enthalpy of crystallization (ΔH_c) were determined from their DSC curves and tabulated in Table 6.

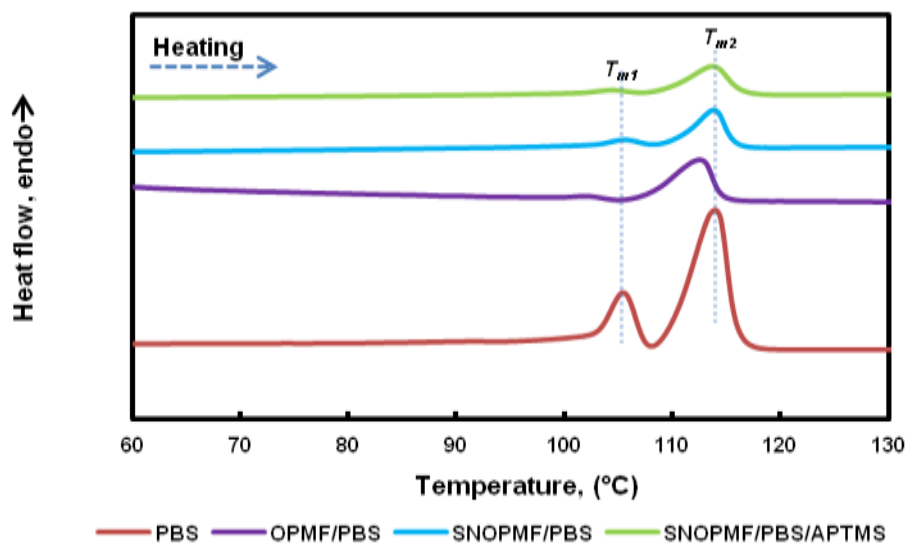


Fig. 11. DSC heating curves of PBS and its biocomposites

As can be seen in Fig. 11, the DSC heating curves of neat PBS showed two endothermic peaks that are attributed to the melting and re-crystallization mechanism (Yasuniwa and Satou 2002). The T_{m1} and T_{m2} of PBS were recorded to be 104.7 and 113.4 °C, respectively, in Table 6. These values decreased to temperatures of 101.0 and 111.9 °C upon the addition of 70 wt.% OPMF (OPMF/PBS). Similarly, the ΔH_m of neat PBS decreased from 57.7 J/g to 10.9 J/g for the OPMF/PBS biocomposite. The decrease in ΔH_m lowered the χ_c value of PBS from 52.3% to 32.9% for the OPMF/PBS biocomposite. The decrease in χ_c value can be related to the low χ_c value of OPMF, which was reported to be around 33.0% in the authors' previous work (Then *et al.* 2014c). Apart from that, the presence of OPMF could also disturb the chain arrangement in PBS, thereby decreasing the χ_c for the corresponding biocomposite.

The pre-treatment of fiber as well as the addition of APTMS only marginally increased the T_{m1} and T_{m2} for the corresponding biocomposites. However, the ΔH_m increased from 10.9 J/g for the OPMF/PBS biocomposite to 17.4 and 18.4 J/g for the SNOPMF/PBS and SNOPMF/PBS/APTMS biocomposites, respectively. The increase in

ΔH_m subsequently caused an increase in the χ_c value of the corresponding biocomposites. The initial χ_c of the OPMF/PBS biocomposite, which was recorded as 32.9%, has substantially increased to 52.6 and 55.5% for the SNOPMF/PBS and SNOPMF/PBS/APTMS biocomposites, respectively. It is well established that crystallinity plays an important role in determining the mechanical properties of composite materials. Therefore, the increase in χ_c may have also triggered the increase in the mechanical properties of the SNOPMF/PBS and SNOPMF/PBS/APTMS biocomposites, as previously discussed in the mechanical properties measurements.

Table 6. Melting Temperature, Enthalpy of Melting, Crystallization Temperature, Enthalpy of Crystallization, and Crystallinity of PBS and its Biocomposites

Sample	T_{m1} (°C)	T_{m2} (°C)	ΔH_m (J/g)	χ_c (%)	T_c (°C)	ΔH_c (J/g)
PBS	104.7	113.4	57.7	52.3	89.5	68.2
OPMF/PBS	101.0	111.9	10.9	32.9	84.9	18.6
SNOPMF/PBS	104.9	113.9	17.4	52.6	86.1	16.0
SNOPMF/PBS/APTMS	104.9	114.1	18.4	55.5	87.7	15.3

An exothermic peak was noted for neat PBS during the cooling scan, as illustrated in Fig. 12. This peak is related to the crystallization of PBS upon cooling. The T_c of neat PBS, initially 89.5 °C, decreased to a temperature of 84.9 °C for the OPMF/PBS biocomposite. The decrease in T_c was attributed to the increase in viscosity of the biocomposite, resulting from the confinement of polymer chains by OPMF that can hinder the migration and diffusion of PBS molecular chains toward the surface during the crystallization process (Terzopoulou *et al.* 2014). The pre-treatment of fiber and the use of APTMS shifted the T_c to higher temperatures of 86.1 and 87.7 °C for the SNOPMF/PBS and SNOPMF/PBS/APTMS biocomposites, respectively. The increase in T_c can be explained by the nucleation effect promoted by the SNOPMF and APTMS. This observation was corroborated by the increase in χ_c for the corresponding biocomposite. The increase in T_c also resulted in a slight reduction of ΔH_c (Table 6).

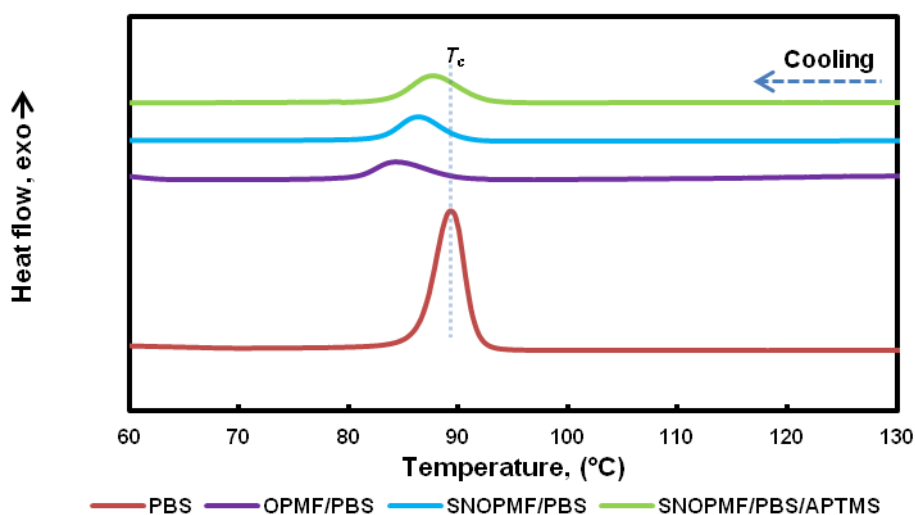


Fig. 12. DSC cooling curves of PBS and its biocomposites

Thermal Stability

The thermal stability of biocomposites was assessed *via* thermogravimetric analysis. The weight loss and derivative weight loss curves with respect to temperature for the OPMF/PBS, SNOPMF/PBS, and SNOPMF/PBS/APTMS biocomposites are illustrated in Figs. 13 and 14, respectively. The information regarding the nature and extent of degradation of the materials, such as the temperatures at which moisture was volatilized from the material and the weight lost due to the thermal degradation process, can be interpreted from the curves. The detailed interpretations of the curves are tabulated in Tables 7 and 8.

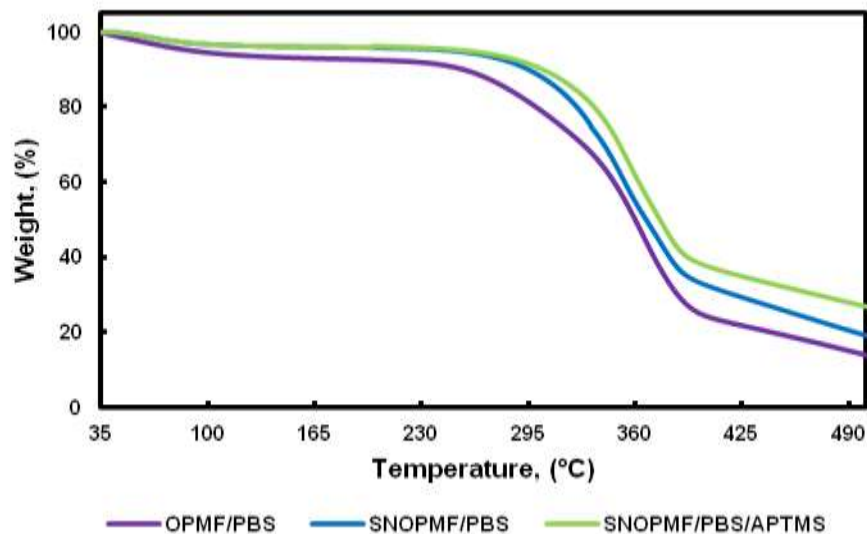


Fig. 13. TG curves of OPMF/PBS, SNOPMF/PBS, and SNOPMF/PBS/APTMS biocomposites

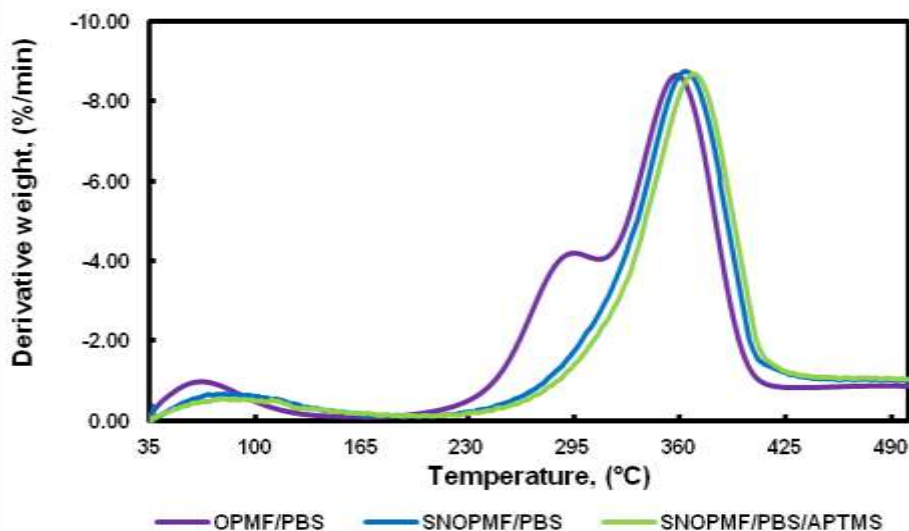


Fig. 14. DTG curves of OPMF/PBS, SNOPMF/PBS, and SNOPMF/PBS/APTMS biocomposites

As can be seen in Figs. 13 and 14, the thermal degradation process of the biocomposites occurred in two to three sequential steps. The first degradation step, within the temperature range of 35.0 to 160.0 °C, was related to moisture evaporation. The OPMF/PBS biocomposite showed the highest weight loss value at 7.07%, and the

SNOPMF/PBS/APTMS biocomposite showed the lowest weight loss value at 2.54%. The reduction in weight loss percentage is attributed to the lower moisture content of SNOPMF in comparison to that of OPMF. In addition, the use of APTMS can result in the formation of chemical linkage between the hydroxyl groups of fiber and the alkoxy groups of APTMS, decreasing the number of hydroxyl groups in SNOPMF to interact with moisture, and thereby decreasing the moisture content for the SNOPMF/PBS/APTMS biocomposite. In this degradation step, the temperature at maximum rate of weight loss (T_{max}), which can be obtained from the peak of the DTG curve, was recorded to be 65.6, 77.9, and 80.1 °C for the OPMF/PBS, SNOPMF/PBS, and SNOPMF/PBS/APTMS biocomposites, respectively. Again, the SNOPMF/PBS/APTMS biocomposite showed higher T_{max} relative to those of the OPMF/PBS and SNOPMF/PBS biocomposites.

Table 7. Temperature at Maximum rate of Degradation (T_{max}) and Weight Loss of Biocomposites

Sample	35-160 °C		160-315 °C		315-500 °C	
	T_{max} (°C)	Weight loss (%)	T_{max} (°C)	Weight loss (%)	T_{max} (°C)	Weight loss (%)
OPMF/PBS	65.6	7.07	295.2	18.02	354.4	61.03
SNOPMF/PBS	77.9	3.48	-	11.78	364.2	65.51
SNOPMF/PBS/APTMS	80.1	2.54	-	8.14	365.6	62.66

As the temperature increased from 160.0 to 315.0 °C, the second degradation step was noted by the presence of a peak at the DTG curve. This step was related to the degradation of the hemicellulose fiber component (Then *et al.* 2014c), and the OPMF/PBS biocomposite showed a weight loss of 18.02% with a T_{max} of 295.2 °C. It is interesting to note that the biocomposites of SNOPMF/PBS and SNOPMF/PBS/APTMS did not show any peak in the DTG curves within this temperature region. This can be explained by the lower percentage of hemicellulose in SNOPMF as compared to that of OPMF and clearly manifested by lower weight loss recorded for the SNOPMF/PBS and SNOPMF/PBS/APTMS biocomposites as compared to the OPMF/PBS biocomposite. The weight loss of 11.78% for the SNOPMF/PBS biocomposite further decreased to 8.14% for the SNOPMF/PBS/APTMS biocomposite. This can be explained by the fact that chemical linkage could be formed between APTMS and fiber (Figs. 7c-d) rendering the fiber more thermally stable and causing the degradation process to occur at a higher temperature.

In the temperature range of 315 to 500 °C, degradations of PBS as well as cellulose and lignin components from fiber occurred simultaneously. The T_{max} and weight loss for the OPMF/PBS, SNOPMF/PBS, and SNOPMF/PBS/APTMS biocomposites were respectively recorded to be 354.4 °C and 61.03%, 364.2 °C and 65.51%, and 365.6 °C and 62.66%. Among the biocomposites, the SNOPMF/PBS/APTMS biocomposite showed the highest T_{max} due to the fact that chemical linkage may form between fiber and thermoplastic and thereby cause the degradation process to occur at a higher temperature. The weight loss of the SNOPMF/PBS biocomposite was notably higher than that of the OPMF/PBS biocomposite but lower than that of the SNOPMF/PBS/APTMS biocomposite. The higher weight loss for the SNOPMF/PBS biocomposite relative to the OPMF/PBS biocomposite is related to the higher percentages of cellulose and lignin in SNOPMF in comparison to OPMF (Table 1), meaning that

more cellulose and lignin were degraded in this temperature range. The weight loss for the SNOPMF/PBS/APTMS biocomposite was slightly lower than that of the SNOPMF/PBS biocomposite and this may again be attributed to the formation of stronger chemical bonding between SNOPMF and PBS in the presence of APTMS, which may hinder the degradation of individual components within the biocomposite, thereby decreasing the weight loss in this temperature region.

Table 8. Thermal Degradation Temperatures of Biocomposites at 5, 10, and 50% Weight Loss and Their Residue at 500 °C

Sample	Temperature °C			Residue at 500 °C, (%)
	$T_{5\%}$	$T_{10\%}$	$T_{50\%}$	
OPMF/PBS	89.3	254.8	359.9	13.88
SNOPMF/PBS	249.1	295.3	366.8	19.23
SNOPMF/PBS/APTMS	256.9	303.6	374.7	26.66

The thermal stability of the biocomposites could also be discussed in terms of the temperatures at which 5, 10, and 50% weight loss ($T_{5\%}$, $T_{10\%}$, and $T_{50\%}$) occurred. As tabulated in Table 8, the SNOPMF/PBS/APTMS biocomposite showed the highest $T_{5\%}$, $T_{10\%}$, and $T_{50\%}$ relative to those of the SNOPMF/PBS and OPMF/PBS biocomposites. For instance, the $T_{10\%}$ for the OPMF/PBS, SNOPMF/PBS, and SNOPMF/PBS/APTMS biocomposites appeared to be 254.8, 295.3, and 303.6 °C, respectively. In this context, higher $T_{10\%}$ is associated with higher thermal stability, therefore the SNOPMF/PBS/APTMS biocomposite showed higher thermal stability relative to the OPMF/PBS and SNOPMF/PBS biocomposites. This result indicates that the use of APTMS is beneficial for improving the thermal stability of biocomposites. On the other hand, the OPMF/PBS, SNOPMF/PBS, and SNOPMF/PBS/APTMS biocomposites showed 13.88, 19.23, and 26.66% residues at 500 °C, respectively. The relatively high percentage of residue for the SNOPMF/PBS and SNOPMF/PBS/APTMS biocomposites may be attributed to the higher lignin content of SNOPMF, as well as the presence of inorganic content (Si) in APTMS, as both components have higher thermal degradation temperatures.

CONCLUSIONS

1. The presence of APTMS enhanced the tensile and flexural properties as well as the impact resistant of SNOPMF/PBS biocomposites due to the enhanced interfacial adhesion between SNOPMF and PBS, as indicated by microscopy observation and short beam shear testing.
2. The resistance to water uptake and thickness swelling of SNOPMF/PBS biocomposites were considerably improved in the presence of APTMS.
3. The FTIR study indicated that chemical bonding was established between the SNOPMF, PBS, and APTMS. The presence of APTMS enhanced the thermal stability and crystallinity of the SNOPMF/PBS biocomposite as demonstrated by thermogravimetric and differential calorimetric analyses, respectively.

ACKNOWLEDGMENTS

The authors would like to acknowledge the Ministry of Education, Malaysia, for the provision of a MyPhD scholarship. The authors wish to thank all technical staff in the Department of Chemistry, Faculty of Science, Universiti Putra Malaysia for their kind assistance.

REFERENCES CITED

- ASTM D2344/D2344M. (2000). "Standard test method for apparent interlaminar shear strength of unidirectional parallel fiber composites by short beam method," American Society of Testing and Materials, West Conshohocken, PA.
- ASTM D256. (2000). "Standard test methods for determining the Izod pendulum impact resistance of plastics," American Society of Testing and Materials, West Conshohocken, PA.
- ASTM D3418. (2008). "Standard test method for transition temperatures and enthalpies of fusion and crystallization of polymers by differential scanning calorimetry," American Society of Testing and Materials, West Conshohocken, PA.
- ASTM D5023. (2009). "Standard test method for plastics: dynamic mechanical properties: in flexure (three-point bending)," American Society of Testing and Materials, West Conshohocken, PA.
- ASTM D570. (2005). "Standard test method for water absorption of plastics," American Society of Testing and Materials, West Conshohocken, PA.
- ASTM D638-5. (2000). "Standard test method for tensile properties of plastics," American Society of Testing and Materials, West Conshohocken, PA.
- ASTM D790. (2000). "Standard test method for flexural properties of unreinforced and reinforced plastics," American Society of Testing and Materials, West Conshohocken, PA.
- Bachtiar, D., Sapuan, S. M., and Hamdan, M. M. (2008). "The effect of alkaline treatment on tensile properties of sugar palm fiber reinforced epoxy composites," *Materials & Design* 29(7), 1285-1290. DOI: 10.1016/j.matdes.2007.09.006
- Basiron, Y. (2007). "Palm oil production through sustainable plantations," *European Journal of Lipid Science and Technology* 109(4), 289-295. DOI: 10.1002/ejlt.200600223
- Bin, T., Qu, J. P., Liu, L. M., Feng, Y. H., Hu, S. X., and Yin, X. C. (2011). "Non-isothermal crystallization kinetics and dynamic mechanical thermal properties of polybutylene succinate composites reinforced with cotton stalk bast fibers," *Thermochimica Acta* 525(1-2), 141-149. DOI: 10.1016/j.tca.2011.08.003
- Dong, S., and Gauvin, R. (1993). "Application of dynamic mechanical analysis for the study of the interfacial region in carbon fiber/epoxy composite materials," *Polymer Composites* 14(5), 414-420. DOI: 10.1002/pc.750140508
- EN317. (2003). "Particleboard and fiberboards; determination of swelling in thickness after immersion in water," European Committee for Standardization, London.
- Eng, C. C., Ibrahim, N. A., Zainuddin, N., Ariffin, H., Wan Yunus, W. M. Z., and Then, Y. Y. (2014). "Enhancement of mechanical and dynamic mechanical properties of hydrophilic nanoclay reinforced polylactic acid/polycaprolactone/oil palm mesocarp

- fiber hybrid composites,” *International Journal of Polymer Science* 2014, 1-8. DOI:10.1155/2014/715801
- Georgopoulos, S. T., Tarantili, P. A., Avgerinos, E., Andreopoulos, A. G., and Koukios, E. G. (2005). “Thermoplastic polymers reinforced with fibrous agricultural residues,” *Polymer Degradation and Stability* 90(2), 303-312. DOI: 10.1016/j.polymdegradstab.2005.02.020.
- Hosseinaei, O., Wang, S., Enayati, A. A., and Rials, T. G. (2012). “Effects of hemicellulose extraction on properties of wood flour and wood-plastic composites,” *Composites Part A: Applied Science and Manufacturing* 43(4), 686-694. DOI: 10.1016/j.compositesa.2012.01.007
- Islam, M. N., Rahman, M. R., Haque, M. M., and Huque, M. M. (2010). “Physico-mechanical properties of chemically treated coir reinforced polypropylene composites,” *Composites Part A: Applied Science and Manufacturing* 41(2), 192-198. DOI: 10.1016/j.compositesa.2009.10.006
- Karmarkar, A., Chauhan, S. S., Modak, J. M., and Chanda, M. (2007). “Mechanical properties of wood-fiber reinforced polypropylene composites: Effect of a novel compatibilizer with isocyanate functional group,” *Composites Part A: Applied Science and Manufacturing* 38(2), 227-233. DOI: 10.1016/j.compositesa.2006.05.005
- Kim, H. S., Kim, H. J., Lee, J. W., and Choi, I. G. (2006). “Biodegradability of bio-flour filled biodegradable poly(butylene succinate) bio-composites in natural and compost soil,” *Polymer Degradation and Stability* 91(5), 1117-1127. DOI: 10.1016/j.polymdegradstab.2005.07.002
- Kim, H. S., Yang, H. S., Kim, H. J., Lee, B. J., and Hwang, T. S. (2005). “Thermal properties of agro-flour-filled biodegradable polymer bio-composites,” *Journal of Thermal Analysis and Calorimetry* 81(2), 299-306. DOI: 10.1007/s10973-005-0782-7
- Lau, H. L. N., Choo, Y. M., Ma, A. N., and Chuah, C. H. (2008). “Selective extraction of palm carotene and vitamin E from fresh palm-press mesocarp fiber (*Elaeis guineensis*) using supercritical CO₂,” *Journal of Food Engineering* 84(2), 289-296. DOI: 10.1016/j.jfoodeng.2007.05.018
- Mohd Sis, A. L., Ibrahim, N. A., and Wan Yunus, W. M. Z. (2013). “Effect of 3 aminopropyltrimethoxysilane on mechanical properties of PLA/PBAT blend reinforced kenaf fiber,” *Iranian Polymer Journal* 22(2), 101-108. DOI: 10.1007/s13726-012-0108-0
- Nekkaa, S., Guessoum, M., Grillet, A. C., and Haddaoui, N. (2012). “Mechanical properties of biodegradable composites reinforced with short *Spartium junceum* fibers before and after treatments,” *International Journal of Polymeric Materials and Polymeric Biomaterials* 61(13), 1021-1034. DOI: 10.1080/00914037.2011.617332
- Nam, T. H., Ogihara, S., Tung, N. H., and Kobayashi, S. (2011). “Effect of alkali treatment on interfacial and mechanical properties of coir fiber reinforced polybutylene succinate biodegradable composites,” *Composites Part B: Engineering* 42(6), 1648-1656. DOI: 10.1016/j.compositesb.2011.04.001
- Pothan, L. A., Oommen, Z., and Thomas, S. (2003). “Dynamic mechanical analysis of banana fiber reinforced polyester composites,” *Composites Science and Technology* 63(2), 283-293. DOI: 10.1016/S0266-3538(02)00254-3
- Pothan, L. A., Thomas, S., and Groeninckx, G. (2006). “The role of fibre/matrix interactions on the dynamic mechanical properties of chemically modified banana fibre/polyester composites,” *Composites Part A: Applied Science and Manufacturing*, 37(9), 1260-1269, DOI: 10.1016/j.compositesa.2005.09.001.

- Ray, D., Das, K., Ghosh, S. N., Bandyopadhyay, N. R., Sahoo, S., Mohanty, A. K., and Misra, M. (2010). "Novel materials from sesame husks and unsaturated polyester resin," *Industrial & Engineering Chemistry Research* 49(13), 6069-6074. DOI: 10.1021/ie1003703
- Sreekala, M. S., Kumaran, M. G., and Thomas, S. (1997). "Oil palm fibers: Morphology, chemical composition, surface modification, and mechanical properties," *Journal of Applied Polymer Science* 66(5), 821-835. DOI: 10.1002/(SICI)1097-4628(19971031)66:5<821::AID-APP2>3.0.CO;2-X
- Teh, C. C., Ibrahim, N. A., and Wan Yunus, W. M. Z. (2013). "Response surface methodology for the optimization and characterization of oil palm mesocarp fiber-graft-polybutyl acrylate" *BioResources* 8(4), 5244-5260. DOI: 10.15376/biores.8.4.5244-5260
- Terzopoulou, Z. N., Papageorgiou, G. Z., Papadopoulou, E., Athanassiadou, E., Reinders, M., and Bikiaris, D. N. (2014). "Development and study of fully biodegradable composite materials based on polybutylene succinate and hemp fibers or hemp shives," *Polymer Composites* [Online first]. DOI: 10.1002/pc.23194
- Then, Y. Y., Ibrahim, N. A., Zainuddin, N., Ariffin, H., and Wan Yunus, W. M. Z. (2013). "Oil palm mesocarp fiber as new lignocellulosic material for fabrication of polymer/fiber biocomposites," *International Journal of Polymer Science* 2013, 1-7. DOI: 10.1155/2013/797452
- Then, Y. Y., Ibrahim, N. A., Zainuddin, N., Ariffin, H., Wan Yunus, W. M. Z., and Chieng, B. W. (2014a). "The influence of green surface modification of oil palm mesocarp fiber by superheated steam on the mechanical properties and dimensional stability of oil palm mesocarp fiber/poly(butylene succinate) biocomposite," *International Journal of Molecular Sciences* 15(9), 15344-15357. DOI: 10.3390/ijms150915344
- Then, Y. Y., Ibrahim, N. A., Zainuddin, N., Ariffin, H., Wan Yunus, W. M. Z., and Abd Rahman, M. F. (2014b). "Effect of electron beam irradiation on the tensile properties of oil palm mesocarp fibre/poly(butylene succinate) biocomposites," *International Journal of Automotive and Mechanical Engineering* 10(July-December), 2070-2080. DOI: 10.15282/ijame.10.2014.23.0174
- Then, Y. Y., Ibrahim, N. A., Zainuddin, N., Ariffin, H., Wan Yunus, W. M. Z., and Chieng, B. W. (2014c). "Surface modifications of oil palm mesocarp fiber by superheated steam, alkali, and superheated steam-alkali for biocomposite applications," *BioResources* 9(4), 7467-7483. DOI:10.15376/biores.9.4.7467-7483
- Then, Y. Y., Ibrahim, N. A., Zainuddin, N., Ariffin, H., Wan Yunus, W. M. Z., and Chieng, B. W. (2015a). "Static mechanical, interfacial, and water absorption behaviors of alkali treated oil palm mesocarp fiber reinforced poly(butylene succinate) biocomposites," *BioResources* 10(1), 123-136. DOI:10.15376/biores.10.1.123-136
- Then, Y. Y., Ibrahim, N. A., Zainuddin, N., Chieng, B. W., Ariffin, H., and Wan Yunus, W. M. Z. (2015b). "Influence of alkaline-peroxide treatment of fiber on the mechanical properties of oil palm mesocarp fiber/poly(butylene succinate) biocomposite," *BioResources* 10(1), 1730-1746. DOI:10.15376/biores.10.1.1730-1746
- Vilaseca, F., Mendez, J. A., Lopez, J. P., Vallejos, M. E., Barbera, L., Pelach, M. A., and Mutje, P. (2008). "Recovered and recycled kraft fibers as reinforcement of PP

- composites,” *Chemical Engineering Journal* 138(1-3), 586-595. DOI: 10.1016/j.cej.2007.07.066
- Wang, L., Zhang, J., Yang, X., Zhang, C., Gong, W., and Yu, J. (2014). “Flexural properties of epoxy syntactic foams reinforced by fiberglass mesh and/or short glass fiber,” *Materials & Design* 55, 929-936. DOI: 10.1016/j.matdes.2013.10.065
- Xie, Y., Hill, C. S. A., Xiao, Z., Militz, H., and Mai, C. (2010). “Silane coupling agent used for natural fiber/polymer composites: A review,” *Composites Part A: Applied Science and Manufacturing* 41(7), 806-819. DOI: 10.1016/j.compositesa.2010.03.005
- Zhao, P., Liu, W. Q., Wu, Q. S., and Ren, J. (2010). “Preparation, mechanical, and thermal properties of biodegradable polyesters/polylactic acid blends,” *Journal of Nanomaterials* 2010, 1-8. DOI:10.1155/2010/287082
- Zhao, Y., Qiu, J., Feng, H., and Zhang, M. (2012). “The interfacial modification of rice straw fiber reinforced poly(butylene succinate) composites: Effect of aminosilane with different alkoxy groups,” *Journal of Applied Polymer Science* 125(4), 3211-3220. DOI: 10.1002/app.36502

Article submitted: January 20, 2015; Peer review completed: April 19, 2015; Revisions received and accepted: April 22, 2015; Published: April 27, 2015.

DOI: 10.15376/biores.10.2.3577-3601